Interactive Visualization of the Cranio-Cerebral Correspondences for 10/20, 10/10 and 10/5 Systems

José Angel Iván Rubianes Silva
Sch. of Elec. and Computer Engineering
University of Campinas
Campinas, Brazil
Email: jairs@dca.fee.unicamp.br

Fabio Enrique Suarez Burgos
School of Medical Science
University of Campinas
Campinas, Brazil
Email: faensubu@hotmail.com

Wu, Shin-Ting
Sch. of Elec. and Computer Engineering
University of Campinas
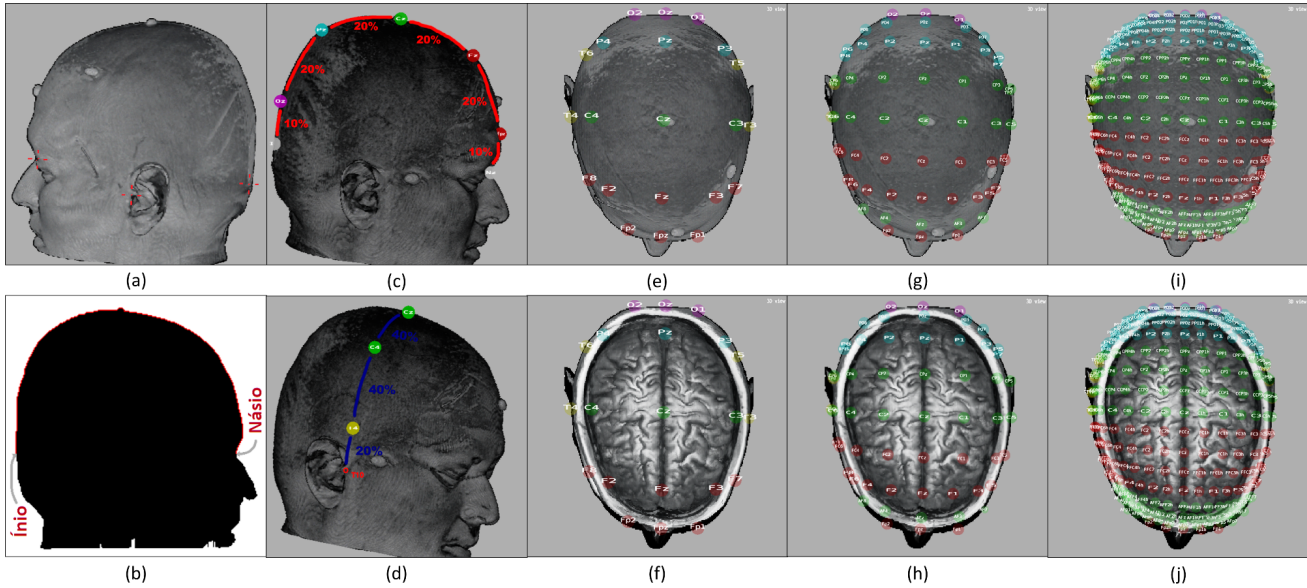Campinas, Brazil
Email: ting@dca.fee.unicamp.br

Fig. 1. Primary reference points, nasion, inion and preauricular ones, are selected on the T1-weighted magnetic resonance volume. They are indicated with a red hair-cross (a). Then, the slice of the head on the midsagittal plane is segmented (b) and the sagittal central reference curve determined (c). This reference curve is divided from nasion to inion in fractions specified by the international system (d). Other reference curves are set in sequence. The locations of EEG electrodes affixed on the scalp in accordance with the international 10/20 (e), 10/10 (g) and 10/5 (i) system are automatically determined. By adjusting the opacity of the cranial bone marrow the correspondences between the electrodes and the cerebral structure is visualizable (f, h and j).

Abstract—Electroencephalogram (EEG) is a method that records electrical activities of the brain. Reliable interpretation of its measurements rely on accurate correspondence of the scalp electrodes and the underlying cortical surface. To standardize comparative studies international 10/20, 10/10 and 10/5 systems for the placement of electrodes have been proposed to specify the locations of scalp EEG sensors under the assumption that there is a consistent correlation between these sites and the structure of the cerebral cortex. However, several studies have demonstrated that the cranio-cerebral correlations vary greatly. For enhancing the electrophysiological analyses, an algorithm is presented in this paper, allowing the multimodal visualization of EEG and magnetic resonance scan in the patient's native space. The key to our solution is twofold: an interactive image-based electrode placement algorithm and an extended GPU-based multimodal raycasting algorithm. Experimental results show that with the present tool one can easily assess the cranio-cerebral correspondences even when the brain tissue is displaced by structural lesions.

Keywords-International 10/5, 10/10, 10/20 systems; EEG and MRI co-registration; GPU-based multimodal rendering; Image processing.

I. INTRODUCTION

Electroencephalogram (EEG) is a safe and painless brain activity test. It is useful in diagnosing several types of brain disorders changing the electrical activities, such as epilepsy [1]. Under the assumption that there is a consistent correspondence between scalp landmarks and the underlying structure of the cortex, international 10/20, 10/10 and 10/5 system the placement of scalp electrodes have been proposed. The "10" and "x" of 10/x stand for the fractions of total front-back and right-left distances between adjacent electrodes, respectively. These systems establish the electrode positions in the context of EEG tests [2], ensuring reproducibility and

standardizing the comparative studies of inter-subject neural activities as well as of intra-subject signals over time.

Due to a wide range of brain dimension, shape, and gyration, several studies have demonstrated that the cranio-cerebral correlations vary largely [3], [4]. Under certain circunstamces, it may not be reliable to use the anatomical landmarks on the head surface for correlating the brain waves with the findings in anatomical images [5]. Increasing the precision in co-locating the scalp electrode positions and the surface of the cortex should improve electrophysiological analyses and detection of brain areas where the electrical signals causing seizures originate [6], [7]. In this paper we address the interactive visualization of the cortical gyri and sulci beneath the scalp electrodes placed according to the international systems in a patient-centered reference system, or in a patient's native space.

Contributions: This paper presents a novel way to visualize the cranio-cerebral correlation individually. A GPU-based implementation of the procedure for the scalp electrode placement described in [3] is proposed, taking into account the individual asymmetry and the anatomical measures. Differently from the previous work, the present method does neither require superficial fiducial electrode markers nor scalp surface reconstruction. The GPU-based raycasting rendering algorithm presented in [8] is extended for rendering the electrode sites over the unveiled cortical surface, so that an expert can easily assess the electrode–cortex correspondences.

We present a GPU-based rendering of the

A. Related work

With the advances in computer and information systems, various placement techniques have been proposed in order to enhance the reliability in the assessment of the correlation between recorded scalp brain waves and the underlying structure of the cortex. We can roughly classify the existing techniques into three categories: fiducial markers matching (landmark based), scalp surface matching (surface matching based) and the international positioning system (IPS based).

The first category consists in placing capsules of water with gadolinium or other substances, that are visible in the magnetic resonance images (MRI), at the electrode sites on the surface of the head before it is scanned [9]. This method requires additional handling and patient compliance. In the second method the scalp surface must be reconstructed from its digitized data including the electrode positions, and be co-registered with the surface segmented from the MRI volume of the head scanned with MRI-visible markers [10]. This method requires additional digitizing of EEG electrode positions and EEG-based surface reconstruction. The third technique is based on the assumption of consistent correlation between the anatomical landmarks and the underlying cortical structure, and internationally recognized 10/20, 10/10, and 10/5 placement systems of scalp electrodes in the context of an EEG exams are established.

Several studies, such as cortical projections [11] and statistical analyses [4], have been conducted to evaluate the accuracy

in the correlation between the cranial landmarks and the cortical structure. Jurcak et al. perform virtual 10/20, 10/10, and 10/5 measurements on the MR images, and propose to add some additional placement rules to IPS to make relative head-surface-based positioning systems more accurate [3]. Based on this work, Giacometti et al. propose a parcellation algorithm. It is based on the parallel planes generated from the primary reference points and the distance fractions specified by the international system [12]. Besides being an approximation of the placement rules proposed by Jurcak et al., multimodal visualization of EEG and MRI data has not been addressed in [12].

B. Problems

For interactively visualizing the correspondence between the electrode locations placed according to the international systems and the underlying cortical surface, a multimodal rendering strategy is devised to display in a single image both the EEG and MRI data. Once the GPU-based raycasting rendering algorithm is a well-established technique for displaying MRI scalar data, the procedure that renders spatial electrode sites is built on its top. However, three problems were identified. First, the electrode locations on the scalp of the patient under study must be determined in accordance with the international systems. Second, the electrode positions must be rendered on the cranial bone marrow in variable opacity, so that the underlying structure of the cortex is visible as illustrated in Fig. 1. Third, the procedure must be performed at interactive frame rates.

Jurcak et al. provide in [3] a thorough description for unambiguous IPS. Hence, the first problem is reduced to its implementation at interactive frame rates. However, when the procedure presented in [3] is developed, three more questions arose: (1) How to identify the four primary reference points illustrated in Fig. 5, nasion (Nz), inion (Iz) and two preauricular points? (2) How to detect the central point (Cz), shown in Fig. 3, for setting the sagittal central reference curve, and (3) How to determine the reference curves on the scalp surface, as depicted in Fig. 8, without resorting to head segmentation?

C. Technique overview

Fig. 2 summarizes the control flow of the proposed algorithm: the phase of placement and the phase of rendering. For highlighting the differences between the present proposal and the technique found in [3], the additional steps are colored in green in the figure. In the phase of placement, the four primary reference points, nasion (Nz), inion (Iz), left preauricular point (LPA) and right preauricular point (RPA), are first detected manually from MRI by an expert. Second, s/he should additionally select a point on the septum pellucidum (S) illustrated in Fig. 5e. Third, with Nz, Iz and S a midsagittal plane is built, and the intersection between this plane and the head surface yields the sagittal central reference curve. Then, other reference curves are successively constructed according to the specification proposed by Jurcak et al. [3]. Finally, the electrode sites are found by partitioning the reference curves

in the fractions defined in the specified IPS. In the phase of rendering, the MRI volume and the depthmap of the closest valid samples with respect to the observer are first rendered. Then, we render the electrodes lying between the observer and the positions recorded in the depthmap along the viewing direction.
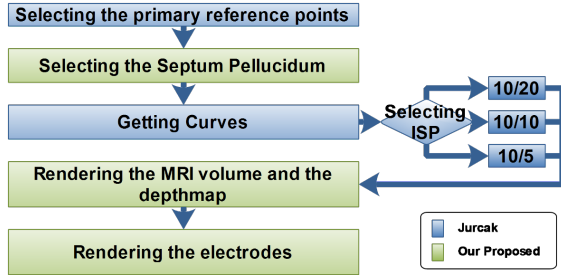

Fig. 2.   Technique overview

To be self-contained, we summarize in Section II some relevant concepts. Then, in Sections III and IV a GPU-based placement and rendering of the scalp electrodes are detailed. The validation experiments and the results are discussed in Sections V and VI. Finally, some concluding remarks are given in Section VII.

II. TECHNICAL BACKGROUND

In this section we present two major concepts that form the basis of the proposed visualization of the EEG International Positioning System.

A. EEG International Positioning System

Correct positioning of the electrodes is crucial for consistent interpretation of the electrical brain waves recorded. Generally, an EEG technician uses conventional tape measures to measure the length between the primary reference points, and to determine the points lying between them in fractions specified by the international 10/20, 10/10 and 10/5 systems [13], as illustrates Fig. 13a.
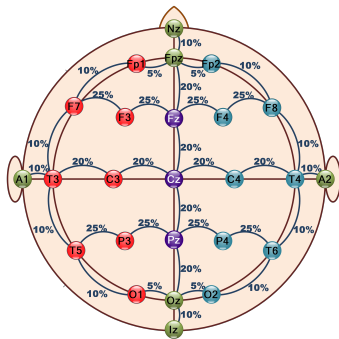

Fig. 3.   10/20 International Positioning System

The International 10/20 System is the most used positioning scheme for EEG exams. It specifies 21 sites on the scalp. They are distributed in such a way that the distances between two adjacent sites along axial reference curve and sagittal central reference curve are, respectively, 10% and 20% of the total front–back and right–left distances of the skull as illustrated in Fig. 3 [14], [15], [16]. The nomenclature of the sensor sites established by the American Clinical Neurophysiology Society (ACNS) facilitates the topographic mapping of EEG activity [17]. Each site is identified by at most two letters and a number. The letters identify the underlying lobes (F(rontal), T(emporal), C(entral), P(arietal)), whereas the numbers indicate the hemisphere location. Even numbers are for the right hemisphere, odd numbers for the left one, and (z)ero refers to electrodes placed along the midline. In addition to these combinations, there are three letter codes A, Pg and Fp that identify the earlobes, nasopharyngeal and frontal polar sites, respectively.

With the development of high resolution EEG for enhancing the tomographic signal source location at the level of the scalp, the 10/20 system is extended to the *The International 10/10 System*. Extra electrodes have been added to fill the sites halfway between those separated by 20% of the total front–back distance in the 10/20 system. To contemplate these new sites new letter codes have been introduced: AF stands for points between Fp and F, FC for those between F and C, FT for those between F and T, CP for those between C and P, TP for those between T and P, and PO for those between P and O. Also, the codes T3/T4 and T5/T6 are renamed to T7/T8 and P7/P8, respectively. Note that in this new nomenclature, except for Fpl/Fp2 and O1/O2, all sites along the same sagittal reference curve have the same number, and those designated by the same letter are laid on the same coronal reference curve. ACNS has accepted as a standard this Modified Combinatorial Nomenclature (MCN) system. It should be noted that, differently from the 10/20 system, the letters do not necessarily refer the underlying cortical region.

Today even higher density electrode settings are commercially available [3]. It is, thus, natural to extend the 10/10 system to the *International 10/5 System* by filling the sites halfway between those separated by 10% of the total front–back distance in the 10/10 system. The new sites receive either a code that contains the letters of its two adjacent sites along the same sagittal reference curve, such as that the site between P7 and PO7 is named as PPO7, or a code ended with "h" when it is halfway of two adjacent sites along the same coronal reference curve.

B. Raycasting Rendering

Raycasting rendering is a well-established GPU-based algorithm for direct volume rendering. It consists in casting a ray from each pixel of the screen towards the scene of interest in the direction of the viewing ray, as presented in Fig. 4. All the samples that intersect the ray, drawn in blue, are mapped onto two graphics attributes, color and opacity [18]. These graphics attributes are accumulated in accordance with the opacity associated to each voxel. The result is a color assigned to the pixel [19]. In the case of the figure, the result is red.

Wu et al. extend this basic procedure in a way that the noise outside the scalp surface is automatically filtered out [8]. In the

place of accumulating all sample contributions of the object of interest along the viewing ray, the accumulation starts after the ray crossing the first sample with the scalar value greater than the user-specified threshold.
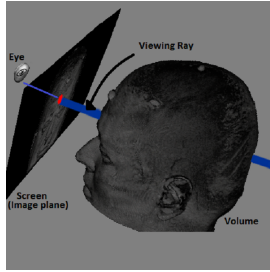

Fig. 4.   Raycasting

III. PROPOSAL

Provided the anatomical MRI volumes, the rules proposed by Jurcak et al. [3] are used to determine unambiguously and individually the electrode sites on the scalp instead of considering the coronal and the sagittal reference curves to be parallel as in [12]. For rendering the electrode sites over the MRI volumes, direct volume rendering technique is applied on MRI and conventional opaque geometry rendering on electrodes. The solutions are proposed in light of two principles: to integrate the potential user in the decision-making process and to simplify the solution by reducing the problem dimensions. The first principle leads to the development of an interactive interface through which an expert interacts with the computer in performing a complex task, while the second conducts to the reduction of 3D problems to 2D ones on which well-known 2D image processing techniques are applicable.
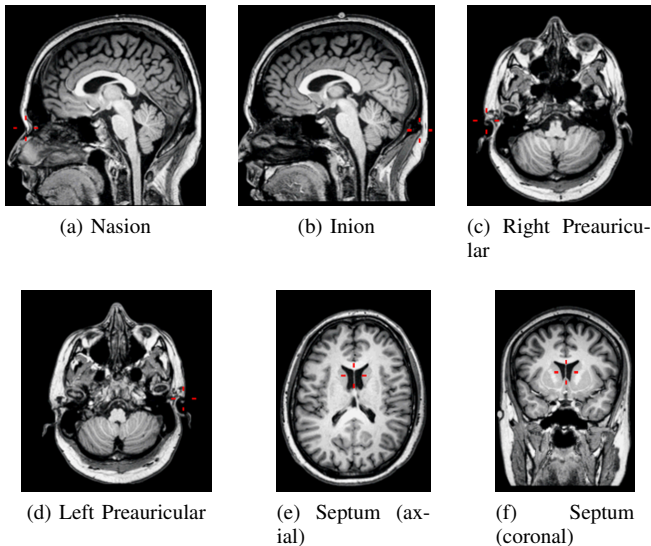

(a) Nasion   (b) Inion   (c) Right Preauricular

(d) Left Preauricular   (e) Septum (axial)   (f) Septum (coronal)

Fig. 5.   Primary reference points.

A. Electrode Positioning

Through a friendly user interface an expert selects manually four primary reference points, nasion (Nz), inion (Iz), left preauricular point (LPA), and right preauricular point (RPA), by pointing on them directly in the displayed MRI volume [20]. In Figs. 5a, 5b, 5c and 5d these points are highlighted with a red cross-hair. Nevertheless, as discussed in [3], one more point is necessary to define the sagittal central reference curve. Instead of taking a point that is equidistant from Nz and Iz and equidistant from the two preauricular points, a novel solution is presented: the user selects a point S on the septum pellucidum as shown in Fig. 5f. Septum pellucidum is a thin membrane located in the midsagittal plane of the brain, between the two cerebral hemispheres, and it is easily detectable in an MRI image.
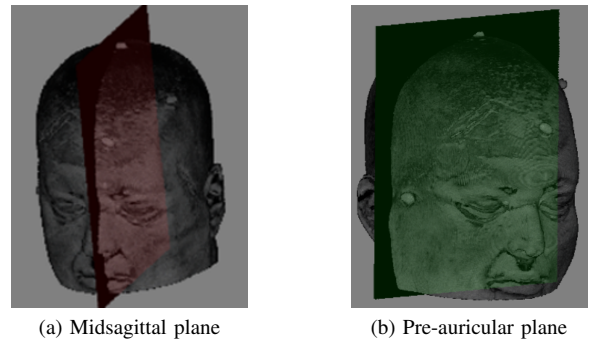

(a) Midsagittal plane   (b) Pre-auricular plane

Fig. 6.   Reference planes.

From Nz, Iz and S we define the midsagittal plane $\mathcal{P}_{\mathcal{MS}}$ (Fig. 6a). The intersection of $\mathcal{P}_{\mathcal{MS}}$ and the scalp yields the sagittal central reference curve. Once the determination of the sagittal central reference curve depends on the scalp surface, it is natural to think that it is necessary to segment the spatial scalp surface from the MRI volume. Instead, we devise a procedure that reduces this 3D image processing problems to a 2D one. The slice of interest is extracted, the noise outside the scalp is filtered out as in Fig. 9b, the image resulted is binarized, and the "white holes" inside the scalp is filled. In this way we get a binary image with a well-defined contour (Fig. 7a), and any edge detection algorithm can be applied to get this contour.

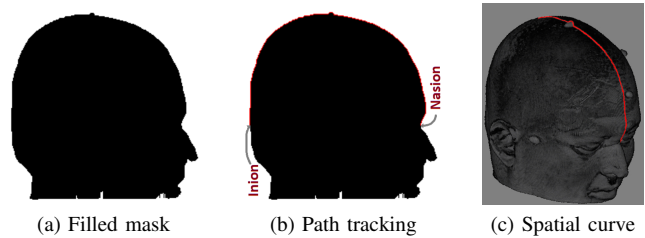(a) Filled mask   (b) Path tracking   (c) Spatial curve

Fig. 7.   Determination of a reference curve.

A gradient-based algorithm is used in the present proposal [21]. The procedure starts from one of the landmarks, ei-

ther nasion or inion, and stops at the other landmark (Fig. 7b). The sequence of n traced edge pixels, $\mathbf{p}_0$, $\mathbf{p}_1$, and $\mathbf{p}_{n-1}$, can be regarded as a piecewise linear approximation of the reference curve that is looked for (Fig. 7c). From $\mathbf{p}_0$, $\mathbf{p}_1$, and $\mathbf{p}_{n-1}$, the arc length of the corresponding reference curve $ArcLength = \sum_{i=1}^{n-1} \|P_i - P_{i+1}\|$ can be estimated and divided in fractions specified by an IPS to obtain the electrode sites. Particularly, in the case of sagittal central reference curve we get the sites Fpz, Fz, Cz Pz and Oz as depicted in Fig. 8a. It should be noted that the midpoint of this sagittal central reference curve coincides with Cz; thus agreeing with the 10/20 IPS (Fig. 3).

The addition of Cz to LPA and RPA enables the building of the pre-auricular plane $\mathcal{P}_{\mathcal{AP}}$, as shown in Fig. 6b. This plane is necessary for getting the coronal central reference curve. Because of the asymmetry of the head, there are measure differences between the left and the right sides of the head. Instead of symmetric parcellation proposed by Giacometti et al. [12], we follow the detailed rules provided in [3] which consists in partitioning with the same fractions specified in light of IPS the differences in the brain hemispheres. Twice the specified fractions on the total arc length are applied in each brain hemisphere along the coronal reference curves. For example, proportions 20%, 40% and 40% are used on the total arc length from the landmark LPA to Cz, and from RPA to Cz. As result, the sites T3 and C3 in the left brain hemisphere (Fig. 8b) and the sites T4 and C4 in the right hemisphere (Fig. 8c) are obtained. This approach guarantees that Cz is the location of an electrode sensor.

(a) NzCzIz   (b) CzA1   (c) CzA2
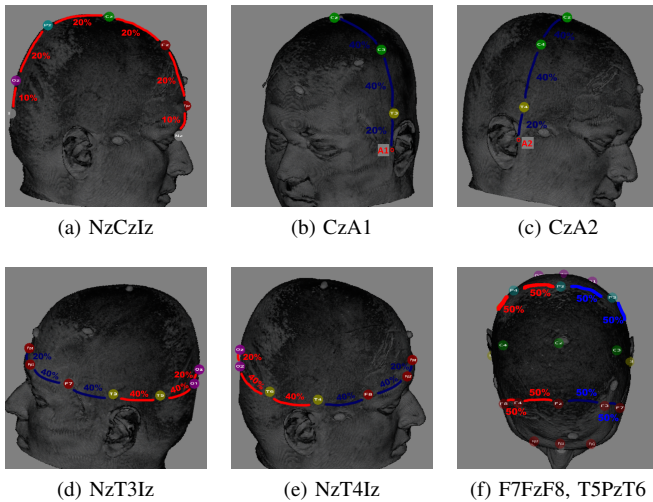
(d) NzT3Iz   (e) NzT4Iz   (f) F7FzF8, T5PzT6

Fig. 8. Reference curves according to the international 10/20 system

With the previously estimated electrode sites, other planes can be built from the rules presented in [3], thus new reference curves. From the plane formed by Fpz, T3 and Oz, the 0% axial reference curve FpzT3OZ whose center does not necessarily match T3 is obtained. The arc T3Fpz is divided at points Fp1 and F7, so that the lengths of the pieces of arc are 40%, 40% and 20% of the total length of T3Fpz, respectively.

Similarly, we divide the arc T3Oz at T5 and O1 sites (Fig. 8d). The method is repeated on the right hemisphere and the sites Fp2, F8, T6 and O2 are determined (Fig. 8e). Finally, we divide the curves PzT5, PzT6, FzF7 and FzF8 in 50% of their lengths for getting P3, P4, F3 and F8 (Fig. 8f).

B. Direct volume and opaque geometry rendering

To visualize the electrode sites and their nomenclature, a sphere textured with the site code is placed on each electrode site, as shown in Fig. 11a. A two stage GPU-based rendering algorithm is elaborated. In the first stage the conventional GLSL-based raycasting shader is performed for rendering the MRI volume. In the second stage the textured spheres are rendered over the image of the MRI volume with the conventional GLSL-based Gouraud shader [18]. Details are provided in Section IV.

IV. IMPLEMENTATION

(a) Raw volume   (b) Filtered volume   (c) Slicing plane

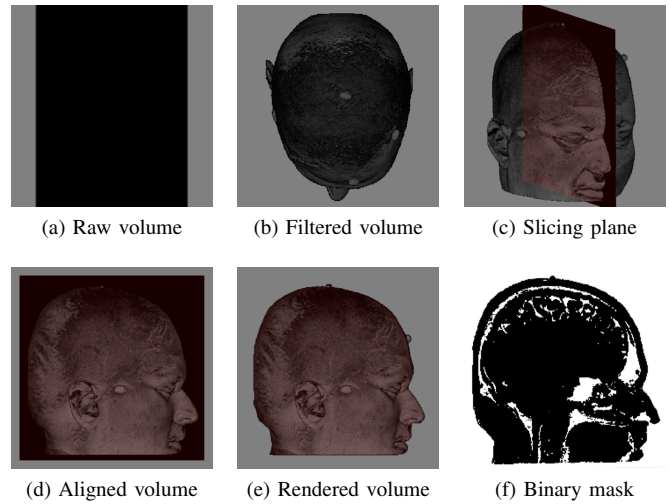(d) Aligned volume   (e) Rendered volume   (f) Binary mask

Fig. 9. Extraction of a slice of interest.

The key to the procedure that segments each reference curve described in Section III-A is to compute the filled mask, illustrated in Fig. 7a, from the raw volume shown in Fig. 9a. Instead of (1) filtering out the noise surrounding the scalp and (2) computing on the CPU the intersection between the filtered volume and the slicing plane that contains the reference curve, an orthogonal view of the raw volume in the direction of the normal vector of the slicing plane is generated with a GLSL shader (Fig. 9c). This is performed as follows. A transformation matrix is applied on the raw volume, so that the normal vector of the plane $\mathcal{P}_{\mathcal{MS}}$ becomes parallel to the view direction. Then, the aligned volume is raycasted (Fig. 9d). Slight modifications in the GPU-based raycasting rendering algorithm described in Section II-B were, however, necessary. Because that only the valid samples that are on the midsagittal plane are of interest, samples are considered "visible" those lying in the neighborhood of the midsagittal plane and with the scalar value above the user-specified threshold. The result is a binary mask with "white" holes, as depicted in Fig. 9f.

Applying a hole-filling algorithm, as the one described in [22] on this binary mask, a filled binary mask shown in Fig. 7a is reached.

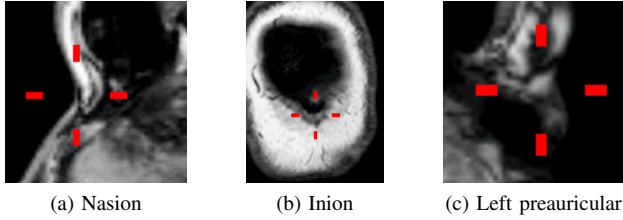(a) Nasion   (b) Inion   (c) Left preauricular

Fig. 10. Identification of primary reference points.

The quality of the selection of primary reference points is crucial for automatic generation of electrode sites. Since its selection is user-dependent, their visual distinction in MRI images is a relevant issue. The nasion is a distinctly depressed area directly between the eyes, just superior to the bridge of the nose (Fig. 10a), and the inion is the most prominent projection of the occipital bone at the lower rear part of the human skull (Fig. 10b). As illustrated in Fig. 10, these prominent geometries are visible in the MRI images. The pre-auriciular points are the points of the posterior root of the zygomatic arch lying immediately in front of the upper end of the tragus. And they are usually difficult to be detected from MRI and can lead to severe misregistration between MRI and EEG [23]. We apply the same strategy proposed in [24] which consists in using the junction between the tragus and the helix. This anatomical landmark can be located much more precisely on the MRI slices as shown in Fig. 10c.

(a) Textured sphere   (b) rendered with depthmap   (c) without depthmap
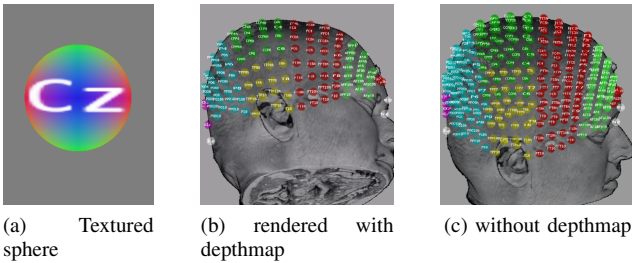
Fig. 11. Multimodal rendering of EEG and MRI.

Finally, to avoid visual clutter of electrodes that are fixed on non-visible side of the scalp in multimodal rendering (Fig. 11c), the electrodes hidden by the patient's head are discarded. The parallel processing power of the GPU is again explored. In the first stage both the MRI image and the depthmap of its visible surface are rendered. This depthmap is applied in the second stage for deciding the visibility of the textured spheres. The spheres that have their depth value less than the values in the depthmap are visible, otherwise they are discarded as shown in Fig. 11b.

Fig. 1 summarizes the results obtained with the proposed technique.

V. EXPERIMENTS

An evaluation of the proposed algorithm was done to assess the timing performance of its implementation based on GPU, its potential in visually providing the cranio-cerebral correlation on an individual basis and at interactive frame rates ([25]), and the precision of the electrode locations generated automatically in comparison with the positions of the electrodes placed manually by an EEG technician. We conducted a series of experiments with brain MRI scans from patients and healthy controls. We remark that all subjects enrolled in the present study signed the informed consent form approved by the Ethics Committee at our university.

First experiment: Concerned about the timing performance we measured variations in the time spent to carry out different tasks as a function of the number of electrode sites, namely the 10/20 (Fig. 1f), 10/10 (Fig. 1h) and 10/5 (Fig. 1j) placement system.

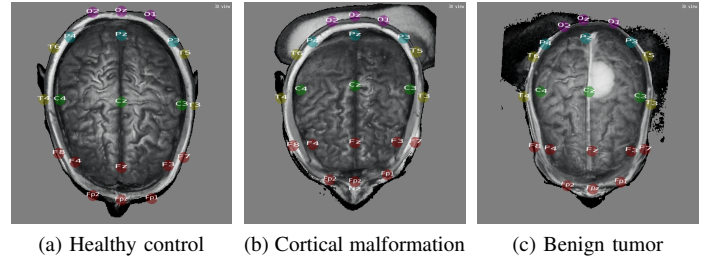(a) Healthy control   (b) Cortical malformation   (c) Benign tumor

Fig. 12. Cranio-cerebral correlation.

Second experiment: Aiming to validate the usefulness of the proposed tool in ascertaining the spatial correlation between the scalp electrodes and the underlying cortical structure, an experiment of the assessment of the correlation between the electrode location and the underlying cortical structure by physicians is designed. We select three representative cases: one healthy control (Fig. 12a), one patient suffering from malformations of cortical development (Fig. 12b) and one patient with a benign tumor (Fig. 12c). In the experiment physicians should only evaluate the correctness of the cortical area underlying each electrode site of the 10/20 system.
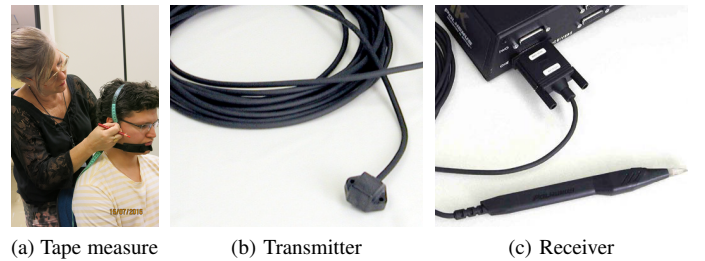

(a) Tape measure   (b) Transmitter   (c) Receiver

Fig. 13. Recording of manual placement of electrodes.

Third experiment: In order to assess the precision of the electrode locations generated automatically by the proposed procedure with respect to the positions of the electrodes

manually placed on the scalp by an EEG technician, an experiment that compares the distances between these two sets of electrode sites is designed. The electrode locations are manually marked with a tape measure by the EEG technician on a volunteer's scalp (Fig. 13a). Then, the markers are recorded by the motion tracker Polhemus Fastrack® consisting of a transmitter generating eletro-magnetic fields (Fig. 13b) and a stylus (receiver) detecting these fields (Fig. 13c). To make the captured positions invariant with respect to the head's movements, the transmitter is fixed on the neck close to the left ear with a black band (Fig. 13a). From the sensed signals the receiver's positions and orientations relative to the transmitter are automatically computed by the tracker. For the purpose of comparison, the coordinates of these positions and orientations should be transformed into the scanned volume's reference system. The matrix that performs this transformation is roughly estimated through four pairs of correspondences provided manually by the user: the 3D position of an anatomical landmark captured by the digitizer's stylus (Fig. 14a) and its correspondence in the scanned volume over which the mouse pointer is hovering (Fig. 14b).

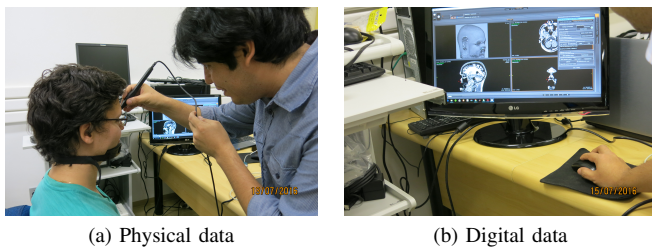(a) Physical data   (b) Digital data

Fig. 14. Input of physical and digital locations of correspondences.

VI. RESULTS AND DISCUSSION

In this section the results achieved in view of performance, visual correlation assessment, precision and limitations are discussed.

A. Performance

Table I lists the timing performance of the present technique on a laptop provided with an Intel processor Core i7–2.00GHz with 8192MB RAM, and a graphics card NVIDIA 820M with 2 GB dedicated VRAM. According to the response time limits in [25], the proposed technique can generate and render IPS-based electrode sites in a response time that a user does not loose the feeling of operating directly on the data. Even for the 10/5 IPS, whose response time is above 1.0s, the response has shown satisfactory in practice. These time responses afford a visual exploration of EEG and MRI correlation.

B. Visual Correlation Assessment

By editing the alpha channel of the transfer function available in the user's interface of the developed prototype, the opacity of the cranial bone marrow is adjustable; thus facilitating the viewing of the correspondence between the electrode locations and the brain cortical surface (Fig. 1 and Fig. 12).

TABLE I
PERFORMANCE TIMES

	International positioning system		
Process (ms)	10/20	10/10	10/5
Calculation of the positions.	459,00	779,00	1479,00
Rendering the electrodes	1,24	114,60	1043,12
Total	460,24	893,60	2522,12

From the neurologist assessment, the electrode sites of the healthy control in Fig. 12a are correctly correlated with the underlying cortical structure. The head's midline and the estimated sagittal central reference curve are visually aligned. However, for the patients that present structural lesions, the correlation between the automatically generated locations of the scalp electrodes and the underlying cortical structure is unpredictable. It will depend on the extent of the lesion and the way that the brain tissue is compressed. In Fig. 12b a small deviation of the sagittal central reference curve from the real medial longitudinal fissure brain can be seen due to the cortical malformations. It causes slight deviation in the cranio-cerebral correspondence. In Fig. 12c the benign tumor compresses the medial longitudinal fissure to left brain hemisphere. Some electrode sites do not have their correspondence to the cortical structure preserved. In these two latter cases, the proposed visualization tool has been shown very useful in providing more accurate co-registration view of the MRI and EEG signals.

C. Precision

Three main measures in quantitative statistics of the distances between automatically computed 10/20 system locations and manually measured positions on the scalp for a male and a female healthy volunteer were calculated. For the male volunteer, they are μ = 58.1mm, σ^2 = 764.0mm^2, and σ = 27.6mm. And for the female volunteer, they are μ = 39.6mm, σ^2 = 350.8mm^2, and σ = 18.7mm. In light of the inaccuracy of the tape measuring, the manual correspondence errors, the unwitting movements of the digitalizer's transmitter, and non-robust estimation of the alignment transformation matrix, these discrepancies are somehow expected. We, however, conjecture that they may be mitigated if more pairs of correspondences are used in the alignment and if we improve the transmitter's fixation system.

D. Limitations

The proposed technique is strongly relied on a high-resolution anatomical MRI scans from which the anatomical landmarks, nasion, inion, preauricular points and septum pellucidum, can be identified. Depending on the clinical cases, not all these landmarks are distinguishable in MRI images. In addition, to automatically segment the reference curves it should require the segmentation of subject's head. We overcome this requirement by applying an in-house developed threshold-based fast segmentation. This technique assumes, however, that the scalp intensity is higher than the noise around the subject's head.

VII. Concluding Remarks

Aiming at interactive exploration of the cranio-cerebral correlation for improving the detection of the focus of abnormal electrical signals that may originate seizures, a GPU-based implementation of the placement procedure proposed by Jurcak et al. [3] is proposed. We show that we may explore the GPU processing features, such as in the scalp segmentation and in the plane–surface intersection, to achieve interactive timing performance as confirmed by the results presented in Section VI-A. From the visual inspection, the correctness in the correspondence of the electrode sites and the underlying cortical structure in the healthy control has been assessed by experts as reported in Section VI-B. This inspection is possible due to interactive adjustments of the opacity of the cranial bone marrow designed. We conclude from our experiment in Section VI-C that the deviations of automatically generated electrode sites from manual expert placements are clinically acceptable in light of the accumulated human errors along the tests. Finally, as pointed in Section VI-D, our algorithm is restricted to reliable identification of the primary reference points and to reliable noise removal. Certainly, there is still room for improvement in the present proposal.

References

[1] HCU, "Electroencefalograma," http://healthcare.utah.edu/healthlibrary/centers/cancer/doc.php?type=92&id=P07655, (Last accessed on 22-01-2016).

[2] Trans Cranial Technologies Ltd., "10/20 System Positioning Manual," p. 20, 2012. [Online]. Available: www.trans-cranial.com

[3] V. Jurcak, D. Tsuzuki, and I. Dan, "10/20, 10/10, and 10/5 systems revisited: Their validity as relative head-surface-based positioning systems," *NeuroImage*, vol. 34, pp. 1600–1611, 2007.

[4] L. Koessler, L. Maillard, A. Benhadid, J. P. Vignal, J. Felblinger, H. Vespignani, and M. Braun, "Automated cortical projection of EEG sensors: Anatomical correlation via the international 10-10 system," *NeuroImage*, vol. 46, no. 1, pp. 64–72, 2009. [Online]. Available: http://dx.doi.org/10.1016/j.neuroimage.2009.02.006

[5] M. Teplan, "Fundamentals of EEG measurement," *Measurement Science Review*, vol. 2, pp. 1–11, 2002.

[6] R. M. F. Fernandes, "O eletrencefalograma na caracterização das síndromes epilépticas," in *Escola Latino-Americana de Verão de Epilepsia: Material Didático*. [Online]. Available: http://www.lasse.med.br/mat_didatico/lasse1/textos/regina01.html

[7] M. S. Beauchamp, M. R. Beurlot, E. Fava, A. R. Nath, N. A. Parikh, Z. S. Saad, H. Bortfeld, and J. S. Oghalai, "The developmental trajectory of brain-scalp distance from birth through childhood: Implications for functional neuroimaging," *PLoS ONE*, vol. 6, no. 9, pp. 1–9, 09 2011. [Online]. Available: http://dx.doi.org/10.1371%2Fjournal.pone.0024981

[8] S.-T. Wu, J. E. Yauri Vidalón, and L. De Souza Watanabe, "Snapping a cursor on volume data," *Proceedings - 24th SIBGRAPI Conference on Graphics, Patterns and Images*, vol. D, no. February, pp. 109–116, 2011.

[9] S. S. Yoo, C. R. G. Guttmann, J. R. Ives, L. P. Panych, R. Kikinis, D. L. Schomer, and F. A. Jolesz, "3D Localization of surface 10-20 EEG electrodes on high resolution anatomical MR images," *Electroencephalography and Clinical Neurophysiology*, vol. 102, no. 4, pp. 335–339, apr 1997. [Online]. Available: http://www.sciencedirect.com/science/article/pii/S0013469496950889

[10] C. Lamm, C. Windischberger, U. Leodolter, E. Moser, and H. Bauer, "Co-registration of EEG and MRI data using matching of spline interpolated and MRI-segmented reconstructions of the scalp surface." *Brain topography*, vol. 14, no. 2, pp. 93–100, 2001. [Online]. Available: http://www.ncbi.nlm.nih.gov/pubmed/11797814

[11] M. Okamoto and I. Dan, "Automated cortical projection of head-surface locations for transcranial functional brain mapping," *NeuroImage*, vol. 26, no. 1, pp. 18–28, may 2005. [Online]. Available: http://dx.doi.org/10.1016/j.neuroimage.2005.01.018

[12] P. Giacometti, K. L. Perdue, and S. G. Diamond, "Algorithm to find high density EEG scalp coordinates and analysis of their correspondence to structural and functional regions of the brain," *Journal of Neuroscience Methods*, vol. 229, pp. 84–96, 2014. [Online]. Available: http://dx.doi.org/10.1016/j.jneumeth.2014.04.020

[13] J. Baztarrica Ochoa, "EEG Signal Classification for Brain Computer Interface Applications," Ph.D. dissertation, Polytechnique, Ecole Lausanne, Federale D E, 2002. [Online]. Available: http://dsp-book.narod.ru/WVT/BZ.pdf

[14] Immrama Institute, "The international 10-20 system of electrode placement," http://www.immramainstitute.com/brainwave-technology-for-health-wellness/eeg-electrode-placement/, (Last accessed on 02-02-2016).

[15] E. Niedermeyer and F. Lopes da Silva, "Electroencephalography: Basic Principles, Clinical Applications, and Related Fields." Lippincott Williams & Wilkins, 2004, ch. 7, p. 140.

[16] K. R. Silva, "Distúrbios paroxisticos não epilépticos-perda de fôlego."

[17] American Clinical Neurophysiology Society, "Guideline 5: Guidelines for Standard Electrode Position Nomenclature," *Clinical Neurophysiology*, vol. 6, pp. 1–3, 2006.

[18] T. T. Elvins, "A survey of algorithms for volume visualization," *ACM Siggraph Computer Graphics*, vol. 26, no. 3, pp. 194–201, 1992.

[19] B. Preim and C. P. Botha, *Visual Computing for Medicine: Theory, Algorithms, and Applications*. Newnes, 2013.

[20] V. Jurcak, M. Okamoto, A. Singh, and I. Dan, "Virtual 10–20 measurement on {MR} images for inter-modal linking of transcranial and tomographic neuroimaging methods," *NeuroImage*, vol. 26, no. 4, pp. 1184 – 1192, 2005. [Online]. Available: http://www.sciencedirect.com/science/article/pii/S1053811905001862

[21] R. K. Mittal and I. J. Nagrath, *Robotics & Control*. Tata McGraw-Hill, 2013. [Online]. Available: http://www.amazon.com/Robotics-Control-MITTAL/dp/0070482934%3FSubscriptionId%3D0JYN1NVW651KCA56C102%26tag%3Dtechkie-20%26linkCode%3Dxm2%26camp%3D2025%26creative%3D165953%26creativeASIN%3D0070482934

[22] P. F. Whela and D. Molloy, *Machine Vision Algorithms in Java: Techniques and Implementation*. Springer, 2000. [Online]. Available: http://www.amazon.com/Machine-Vision-Algorithms-Java-Implementation-ebook/dp/B000QCS4GY%3FSubscriptionId%3D0JYN1NVW651KCA56C102%26tag%3Dtechkie-20%26linkCode%3Dxm2%26camp%3D2025%26creative%3D165953%26creativeASIN%3DB000QCS4GY

[23] D. T. L. L.-C. MD, C. M. M. R. RST, and R. B. M. R. E. T, *Fundamentals of Sleep Technology*. LWW, 2012. [Online]. Available: http://www.amazon.com/Fundamentals-Sleep-Technology-Teofilo-Lee-Chiong/dp/1451132034%3FSubscriptionId%3D0JYN1NVW651KCA56C102%26tag%3Dtechkie-20%26linkCode%3Dxm2%26camp%3D2025%26creative%3D165953%26creativeASIN%3D1451132034

[24] "Coordinatesystems - brainstorm," http://neuroimage.usc.edu/brainstorm/CoordinateSystems, (Accessed on 02/19/2016).

[25] J. Nielsen, "Response time limits: Article by jakob nielsen," https://www.nngroup.com/articles/response-times-3-important-limits/, jun 2010, (Accessed on 19-05-2016).